

CO₂ + CH₄ Chemistry over Pd: Results of Kinetic Simulations Relevant to Environmental Issues

Harrell Sellers, IBM Systems and Technology Group, Rochester, MN
Raymond J. Spiteri, Department of Computer Science, University of Saskatchewan,
Saskatoon, CA
Michael Perrone, IBM Watson Research Center, Yorktown Heights, NY.

Abstract

We have determined the Arrhenius rate constants for 99 chemical reactions on palladium and solved the tightly coupled differential equations describing the chemical kinetics at a number of temperatures ranging from 350K to 700K. The rate equations were integrated to a week of reactor run-time. In this work we discuss the valuable insights that can be gained by closely examining the chemistry ongoing on the first differential slice of the plug flow reactor.

The two-component feed gas consisted of CO₂ and CH₄ with total pressure of 1 bar. The CO₂ – CH₄ partial pressures employed ranged from 20% - 80% to 80% - 20%. In these temperature and pressure ranges, the system performs in the low-coverage regime.

In addition to the feed gas, formaldehyde, methanol, molecular hydrogen, C₂ hydrocarbons, formic acid, acetic acid, ketene, water, and carbon monoxide evolve from the catalyst surface in the first differential slice of the plug flow reactor. The relative amounts of the desorbing reaction products are dependent on the operating temperature and the relative pressures. The results of our simulations are consistent with results reported in the experimental literature.

I. Introduction

Carbon dioxide and methane chemistry over palladium has attracted interest in recent years [1-6]. Gredig et al. [1] have reported the synthesis of methyl amines from CO₂, hydrogen, and NH₃ over palladium under a total pressure of 0.6 MPa in the temperature range of 473 – 573 K. They also report that methane synthesis dominates at temperatures above 573 K. Ding et al. [2] considered the synthesis of acetic acid over supported Pd catalysts from methane and carbon dioxide. They observed formic acid production on palladium with no apparent deactivation resulting from carbon deposition on the catalyst surface.

The term, reforming of methane, is often applied to the reaction between methane and water to form CO and molecular hydrogen (methane is ‘reformed’ to synthesis gas or ‘syngas’). Rezaei et al. [3] reported the production of syngas by methane reforming on a number of transition metal surfaces. They attribute the relatively low efficacy of Pd for the syngas production by methane reforming to carbon deposits on the surface and sintering of the catalyst. Wilcox et al. [5] also considered acetic acid synthesis over supported Pd catalysts as Ding et al. [2] did later. Acetic acid production was observed [5] on 5% Pd on C and 5% Pd on alumina at 400 °C. Munera et al. [6] studied the production of hydrogen from the CO₂ reforming of methane and considered the differences in efficacy between a plug flow reactor and a membrane reactor.

The carbon dioxide / methane chemistry on catalytic surfaces is a rich chemistry involving many small molecules and radicals composed of carbon, hydrogen, and oxygen. Understanding the chemistry of methane and carbon dioxide on catalytic surfaces is relevant to the effort to minimize carbon dioxide emissions from large point sources such as coal-fired electrical generating stations and ethanol production facilities. Carbon dioxide, which is a very stable gas-phase molecule, can be an effective oxygen source for surface reactions in certain situations. Even in the gas-phase for example the reaction between CO_2 and CH_4 yielding graphite and water is thermodynamically favorable at room temperature ($\Delta G^\circ = -29 \text{ kJ/mol}$). One can see that CO_2 can be an effective oxygen source depending on the stability of the products.

In this work we present results obtained from our computational model of the first differential slice of a plug flow Pd reactor employing CO_2 and CH_4 as the two-component feed gas. We discuss the predicted surface coverages and reactor products and the variations with temperature in the range of 350 to 700 K. We also discuss the total and partial pressure dependence of these quantities.

II. The Computational Model

A supported or powder catalyst that is in thermodynamic equilibrium will have surfaces of low Gibbs energy of formation exposed. Certainly at elevated temperatures or under other conditions that allow surface reconstruction, the surfaces of low Gibbs energy of formation will dominate as the exposed catalytic surfaces. Early on in our efforts to

model industrial catalytic processes we ran simulations employing several surfaces of low Gibbs energy of formation. We found that the chemistry of all the low Gibbs energy surfaces is similar. In this work we employ the surface of lowest Gibbs energy of formation, the fcc (111) surface, as the model surface. This strategy has worked very well for us in the past [10].

The accuracy of the UBI-QEP rate constant parameters is difficult to assess. In cases in which reliable experimental values are available, the results of the UBI-QEP method usually agree well [7]. However, the lack of high-quality experimentally derived rate constant parameters limits the extent to which we can compare our results to experimentally derived results. Ultimately the quality of the computational model has to be judged by the quality of the model predictions. It is therefore critical that we make comparisons with experimentally derived data whenever possible.

Figure 1 is a diagram of the cylindrical plug flow reactor. The feed gas enters the reactor from one end, and the products exit from the other. Surface coverages of adsorbed species and gas-phase concentrations change in the axial direction but are presumed to be homogeneous in the radial direction. The plug flow reactor is divided into differential slices to be stacked to complete the mathematical description of the reactor along the axial coordinate.

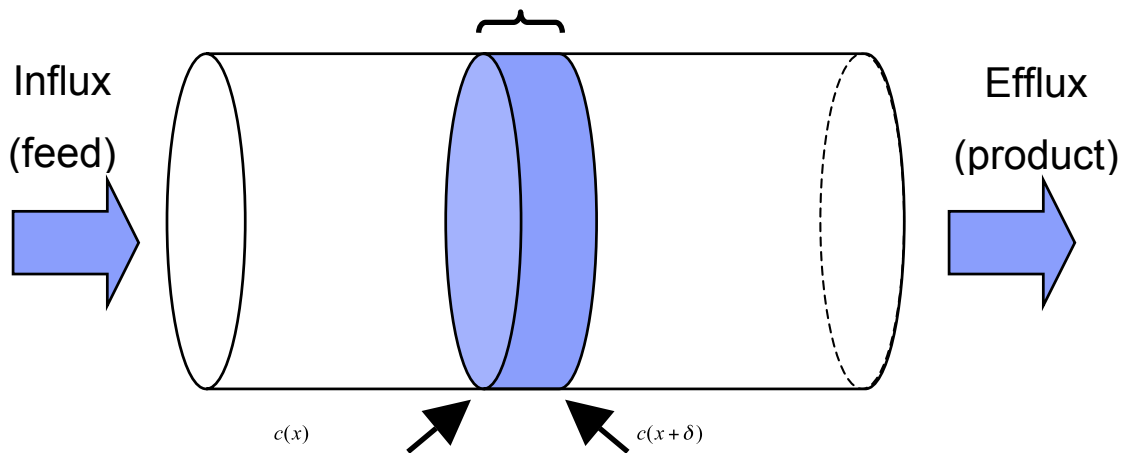


Figure 1. Plug flow reactor.

The output of the first differential slice is the input for the second, and so on. The results presented herein are obtained with a feed gas that is composed of CO_2 and CH_4 . The feed gas composition for any given set of operating parameters (temperature and pressure) does not change. The gases that evolve from the catalyst surface do not become part of the feed gas for the present differential slice. This model is consistent with the first differential slice of the plug flow reactor having a fixed carbon dioxide and methane feed gas composition. The plug-flow reactor is an idealization and one that is employed often in industrial situations.

Development of the kinetic model for the stacked differential slices is presently underway. We expect to see that the chemistry that occurs on subsequent differential slices will approximate that of the first, but there will be differences for which the complete reactor model will account. In this work we examine closely the ongoing chemistry of the first differential slice of the plug flow reactor.

Excluding adsorption and desorption processes, the reacting surface mechanism involves 99 chemical reactions. These are forward and reverse reaction pairs unless the activation barrier of a reaction was high enough to consider that reaction channel to be closed.

Table I contains the reactions and Arrhenius rate constant parameters we employed in this work.

Table I. Reactions, reaction enthalpies, and activation barriers (kcal/mol) on the Pd(111) surface

Reaction/Class	ΔH	ΔE_f	ΔE_r
Atomic Hydrogen Sources			
$\text{CH}_4 \rightarrow \text{CH}_3 + \text{H}$	14.6	19.9	5.3
$\text{CH}_3 \rightarrow \text{CH}_2 + \text{H}$	-0.6	19.3	19.9
$\text{CH}_2 \rightarrow \text{CH} + \text{H}$	7.5	23.3	15.9
$\text{CH} \rightarrow \text{C} + \text{H}$	-34.8	4.9	39.8
$\text{H}_2 \rightarrow \text{H} + \text{H}$	-13.2	8.9	22.1
First Hydrogenation of CO_2			
$\text{CO}_2 + \text{H} \rightarrow \text{OCOH}$	-2.1	0.74	2.9
$\text{CO}_2 + \text{CH}_4 \rightarrow \text{OCOH} + \text{CH}_3$	12.5	18.4	5.9
$\text{CO}_2 + \text{CH}_3 \rightarrow \text{OCOH} + \text{CH}_2$	28.6	30.4	1.8
$\text{CO}_2 + \text{CH}_2 \rightarrow \text{OCOH} + \text{CH}$	5.3	21.1	15.8
$\text{CO}_2 + \text{CH} \rightarrow \text{OCOH} + \text{C}$	-36.9	2.4	39.3
Second Hydrogenation of CO_2			
$\text{OCOH} + \text{H} \rightarrow \text{CO} + \text{H}_2\text{O}$	-4.6	12.5	17.1
$\text{OCOH} + \text{H} \rightarrow \text{HCOOH}$ (formic acid)	19.3	24.4	5.1
$\text{OCOH} + \text{CH}_4 \rightarrow \text{CO} + \text{H}_2\text{O} + \text{CH}_3$	9.0	14.8	5.8
$\text{OCOH} + \text{CH}_3 \rightarrow \text{CO} + \text{H}_2\text{O} + \text{CH}_2$	-19.5	5.1	24.6
$\text{OCOH} + \text{CH}_2 \rightarrow \text{CO} + \text{H}_2\text{O} + \text{CH}$	3.0	16.1	13.1
$\text{OCOH} + \text{CH} \rightarrow \text{CO} + \text{H}_2\text{O} + \text{C}$	-37.5	0	37.5
$\text{OCOH} + \text{CH}_4 \rightarrow \text{HCOOH} + \text{CH}_3$	33.9	33.9	0
$\text{OCOH} + \text{CH}_3 \rightarrow \text{HCOOH} + \text{CH}_2$	50.0	50.0	0
$\text{OCOH} + \text{CH}_2 \rightarrow \text{HCOOH} + \text{CH}$	26.7	26.7	0
$\text{OCOH} + \text{CH} \rightarrow \text{HCOOH} + \text{C}$	-15.6	0	15.6
First Hydrogenation of CO			
$\text{CO} + \text{H} \rightarrow \text{COH}$	24.3	24.3	0

$\text{CO} + \text{H} \rightarrow \text{HCO}$	16.4	18.4	1.5
$\text{CO} + \text{CH}_4 \rightarrow \text{COH} + \text{CH}_3$	38.9	38.9	0
$\text{CO} + \text{CH}_3 \rightarrow \text{COH} + \text{CH}_2$	55.0	55.0	0
$\text{CO} + \text{CH}_2 \rightarrow \text{COH} + \text{CH}$	31.7	34.3	2.6
$\text{CO} + \text{CH} \rightarrow \text{COH} + \text{C}$	-10.6	15.6	26.1
$\text{CO} + \text{CH}_4 \rightarrow \text{HCO} + \text{CH}_3$	31.1	31.1	0
$\text{CO} + \text{CH}_3 \rightarrow \text{HCO} + \text{CH}_2$	47.1	47.1	0
$\text{CO} + \text{CH}_2 \rightarrow \text{HCO} + \text{CH}$	23.9	30.9	7.0
$\text{CO} + \text{CH} \rightarrow \text{HCO} + \text{C}$	-18.0	12.3	30.8

Second Hydrogenation of CO

$\text{COH} + \text{H} \rightarrow \text{H}_2\text{O} + \text{C}$	-135	0	135
$\text{HCO} + \text{H} \rightarrow \text{H}_2\text{CO}$	7.7	16.8	9.1
$\text{COH} + \text{CH}_4 \rightarrow \text{H}_2\text{O} + \text{CH}_3 + \text{C}$	-131.9	0	131.9
$\text{COH} + \text{CH}_3 \rightarrow \text{H}_2\text{O} + \text{CH}_2 + \text{C}$	-160.9	0	160.9
$\text{COH} + \text{CH}_2 \rightarrow \text{H}_2\text{O} + \text{CH} + \text{C}$	-107.4	0	107.4
$\text{COH} + \text{CH} \rightarrow \text{H}_2\text{O} + 2\text{C}$	-180.1	0	180.1
$\text{HCO} + \text{CH}_4 \rightarrow \text{H}_2\text{CO} + \text{CH}_3$	36.7	36.7	0
$\text{HCO} + \text{CH}_3 \rightarrow \text{H}_2\text{CO} + \text{CH}_2$	52.8	52.8	0
$\text{HCO} + \text{CH}_2 \rightarrow \text{H}_2\text{CO} + \text{CH}$	29.5	29.5	0
$\text{HCO} + \text{CH} \rightarrow \text{H}_2\text{CO} + \text{C}$	-12.8	12.6	25.4
$\text{HCO} + \text{CH}_3 \rightarrow \text{CH}_3\text{CHO}$	23.3	24.0	0.7
$\text{COH} + \text{CH}_4 \rightarrow \text{H}_2\text{O} + \text{CCH}_3$	-60.1	0	60.1
$\text{COH} + \text{CH}_3 \rightarrow \text{H}_2\text{O} + \text{CCH}_2$	16.0	22.0	6.0
$\text{COH} + \text{CH}_2 \rightarrow \text{H}_2\text{O} + \text{CCH}$	26.7	29.3	2.6
$\text{COH} + \text{CH} \rightarrow \text{H}_2\text{O} + \text{CC}$	85.0	85.0	0

Dissociation of COOH

$\text{OCOH} \rightarrow \text{CO} + \text{OH}$	22.4	22.4	0
---	------	------	---

Recombination of water

$\text{OH} + \text{H} \rightarrow \text{H}_2\text{O}$	-26.9	0	26.9
---	-------	---	------

Formation of C2 hydrocarbons

Recombination of acetylene

$\text{CH} + \text{CH} \rightarrow \text{C}_2\text{H}_2$	-33.0	10.1	43.1
--	-------	------	------

Recombination of ethylene

$\text{CH}_2 + \text{CH}_2 \rightarrow \text{C}_2\text{H}_4$	-38.8	0	38.8
--	-------	---	------

Recombination of ethane

$\text{CH}_3 + \text{CH}_3 \rightarrow \text{C}_2\text{H}_6$	-15.2	3.0	18.2
--	-------	-----	------

Formation of C₂ radicals

$\text{COH} + \text{CH}_4 \rightarrow \text{H}_2\text{O} + \text{CCH}_3$	-60.1	0	60.1
$\text{COH} + \text{CH}_3 \rightarrow \text{H}_2\text{O} + \text{CCH}_2$	16.0	22.0	6.1

$\text{COH} + \text{CH}_2 \rightarrow \text{H}_2\text{O} + \text{CCH}$	26.7	29.3	2.6
$\text{C} + \text{CH}_3 \rightarrow \text{CCH}_3$	14.7	24.1	9.4
$\text{C} + \text{CH}_2 \rightarrow \text{CCH}_2$	-10.3	20.4	30.7
Hydrogenation of C_2 hydrocarbons			
Atomic hydrogen as the hydrogen source			
$\text{H} + \text{C}_2\text{H}_2 \rightarrow \text{C}_2\text{H}_3$	-21.1	0	21.1
$\text{H} + \text{C}_2\text{H}_3 \rightarrow \text{C}_2\text{H}_4$	0.7	16.0	15.3
$\text{H} + \text{C}_2\text{H}_4 \rightarrow \text{C}_2\text{H}_5$	-4.2	3.3	7.5
$\text{H} + \text{CHCH}_3 \rightarrow \text{C}_2\text{H}_5$	-14.5	9.9	24.5
$\text{H} + \text{C}_2\text{H}_5 \rightarrow \text{C}_2\text{H}_6$	-7.8	8.9	16.7
Hydrogenation via disproportionation			
$\text{CH}_3 + \text{C}_2\text{H}_5 \rightarrow \text{CH}_4 + \text{CHCH}_3$	-0.1	6.0	6.1
$\text{CH}_3 + \text{CHCH}_3 \rightarrow \text{CH}_4 + \text{CCH}_3$	-15.8	5.8	21.6
$\text{CH}_3 + \text{CCH}_3 \rightarrow \text{CHCH}_3 + \text{CH}_2$	17.8	27.9	10.1
$\text{H}_2 + \text{CCH}_3 \rightarrow \text{CHCH}_3 + \text{H}$	-12.1	11.2	23.3
Recombination of C_2			
$\text{C} + \text{C} \rightarrow \text{C}_2$	175	175	0
Disproportionation of CO			
$\text{CO} + \text{CO} \rightarrow \text{CO}_2 + \text{C}$	26.6	26.6	0
Formation of C_4 hydrocarbons			
$2 \text{CCH}_3 \rightarrow \text{H}_3\text{CCCCH}_3$	-17.7	17.6	35.3
$2 \text{CCH}_2 \rightarrow \text{H}_2\text{CCCCH}_2$	-23.2	8.0	31.2
Reactions involving C/O compounds and precursors			
$\text{CH}_2 + \text{CO} \rightarrow \text{CH}_2\text{CO}$	13.2	17.4	4.1
$\text{CH}_3 + \text{CO}_2 \rightarrow \text{CH}_3\text{O} + \text{CO}$	10.4	14.0	3.7
$\text{CH}_3\text{O} + \text{H} \rightarrow \text{CH}_3\text{OH}$	-10.6	7.4	18.0
$\text{CH}_3\text{O} + \text{CH}_4 \rightarrow \text{CH}_3\text{OH} + \text{CH}_3$	-4.0	6.4	2.4
$\text{CH}_3\text{O} + \text{CH}_3 \rightarrow \text{CH}_3\text{OH} + \text{CH}_2$	6.0	7.8	1.8
$\text{CH}_3\text{O} + \text{CH}_2 \rightarrow \text{CH}_3\text{OH} + \text{CH}$	-3.2	12.0	15.2
$\text{CH}_3\text{O} + \text{CH} \rightarrow \text{CH}_3\text{OH} + \text{C}$	-45.5	0	45.5
$\text{CH}_3\text{O} + \text{C} \rightarrow \text{CH}_3 + \text{CO}$	-36.9	0	36.9
$\text{CH}_2\text{O} + \text{CO} \rightarrow \text{CO}_2 + \text{CH}_2$	14.0	14.0	0
$\text{CH}_3\text{COOH} \rightarrow \text{CH}_3 + \text{OCOH}$	-17.7	3.3	21.0
$\text{CH}_3\text{COOH} + \text{H} \rightarrow \text{CH}_3 + \text{HCOOH}$	-4.1	2.7	6.8

The surface reaction energetics were obtained from the UBI-QEP method [7, 8]. The Arrhenius prefactors were obtained from statistical mechanical considerations [8]

together with the Trouton's Rule for small molecule adsorption and desorption [8 – 10].

The heats of adsorption employed in this work are given in Table I.1.

Table I.1. Heats of adsorption on Pd (kcal/mol) for species employed in this work.

Species	ΔH_{ads}
H	62.0
O	87.2
C	160.0
CO	30.2
CO ₂	3.8
CH ₄	14.3
CH ₃	42.5
CH ₂	74.9
CH	106.3
CH ₃ CH ₃	10.2
CH ₂ CH ₃	43.7
CHCH ₃	77.3
CCH ₃	105.8
CCH ₂	78.3
CCH	75.7
CC	28.8
CH ₂ CH ₂	13.2
CHCH ₂	63.1
CHCH	14.9
CH ₃ OH	11.1
CH ₃ O	42.8
CH ₂ O	11.8
CH ₃ CHO	20.6
CH ₂ CHO	74.9
CH ₂ CO	13.6
CH ₃ COOH	11.2
CH ₃ COO	12.8
HCOOH	16.8
OCOH	56.4
HCO	59.0
COH	88.8
H ₂ O	10.1
H ₂	6.6

In this work we modeled adsorption as Langmuir isotherms [11, 12]. All barriers to adsorption were zero. The barriers to desorption were taken to be the heat of adsorption of the desorbing species as determined by the UBI-QEP method. The adsorption and desorption rate constants were determined employing equations 51 and 52 of ref. 8. The Arrhenius prefactors for second order reactions were obtained from equation 27 of ref. 8 and the first order prefactors were obtained from equations 27 and 54 of ref. 8.

The UBI-QEP expression for the disproportionation reaction, $A + BC \rightarrow AB + C$, was derived within the UBI-QEP framework as a type of dissociation reaction [7]. For the disproportionation reaction leading to a three component set of products, we developed the reaction barrier from similar considerations. Additionally, we generalized the UBI-QEP method to include any number of bond indices in the bond index constraint [16]. For this project we expanded this generalization to include the reaction: $AB + CD \rightarrow BD + A + C$. Both approaches gave similar results for reactions between COH and CH_x yielding three product species. However in this work, these reactions do not seem to be important to the overall chemistry.

The proportion of adsorbate collisions with the surface that successfully lead to adsorption is the sticking probability. The mechanism of adsorption involves the process of energy transfer as the incoming adsorbate impacts the surface. Since it impacts the surface with more energy than it needs to immediately desorb, its kinetic energy must be dampened via collisions with other surface species and the surface itself. Our

presumption herein that the barrier to adsorption is zero does not impact the sticking probability. In our model the surface coverages arise from a competition among adsorption, desorption and reaction processes.

The first- and second-order surface reaction rate equations were formulated in coverage units. Third- and higher-order reactions were not considered because three-body and higher collisions have a vanishingly small probability. As a way to keep track of the space available on the surface for reactants and products, the total coverages in ontop, bridge, and hollow binding sites were monitored, and the binding sites themselves were considered on an equal footing with reactants. However, this technique had no effect on the results because, under the prevailing reaction conditions, the reactor runs in the low-coverage regime. Microvariations in coverages over regions of the surface were not considered; this is tantamount to a presumption that surface coverages are homogeneous.

The computational model has a differential equation for each of the adsorbed species. In this model there are 31 surface adsorbed species and 99 surface chemical reactions. For a given temperature, feed gas composition and total pressure, the rate equations were integrated to a run-time of one week using the ode15s solver in Matlab because the resulting set of differential equations was stiff. ode15s is a variable-stepsize variable-order linear multistep solver based on a modification of the classical backward differentiation formulas known as the numerical differentiation formulas [13]. Steady state was generally achieved early in the runtime.

III. Discussion

Figure 2 displays the surface coverages from 350K to 700K, and Figure 3 is a graph of the total amount of desorbed species in coverage units. Although the absolute coverages are small, the predominant adsorbates are the strongly bound radicals except for CO. The general trend is for the radical coverages to be greater at higher temperatures.

A point we emphasize is regarding the akinetic view of surface reactions [8].

Practitioners of the akinetic view seek to understand what is on the surface based on knowledge of the heats of adsorption. Reaction kinetics are not taken into account, and predictions of product formation are based on knowledge of the activation barriers and estimates of surface coverages. Complex competitions among reactions can not be taken into account in the akinetic view. As was our experience in modeling the Phillips Petroleum acetylene hydrogenation catalyst [8], conjectures appearing in the literature based on adsorbate binding energies regarding surface coverages turned out to be inaccurate.

The relative prominence of the adsorbate CH_3 in Figure 2 is suggestive that the C_2 hydrocarbons should be present in the effluent stream. This is depicted in Figure 3. The C_2 hydrocarbons, acetylene, ethylene, and ethane are desorbing species. The desorbing closed-shell molecules are weakly bound to the surface. They rarely have a significant surface coverage, the exceptions being the components of the feed gas. Figure 3 lists the

closed-shell molecules produced in this reaction mechanism with the total amount that has desorbed at one week of run-time.

Formic acid has been shown to be reactive on the Pd(110) surface, decomposing to CO, CO₂, H₂, and water during TPD (temperature programmed desorption) experiments at 140K [14]. The shortest route to formic acid in our model, which begins with CO₂ and CH₄, is through the first and second hydrogenation of CO₂. This route involves the reactive intermediate OCOH, which is formed in several ways. The disproportionation of CO₂ with CH_x species, $x > 1$, produces OCOH with activation barriers between 18 and 30 kcal/mol. The OCOH radical is also produced by reacting CO₂ with atomic hydrogen with a reaction activation barrier of 0.7 kcal/mol. With atomic hydrogen as the hydrogen source, the formation of OCOH is favored over the reverse reaction. With CH_x species as the hydrogen source, the back reactions have lower barriers with the exception of $x = 1$.

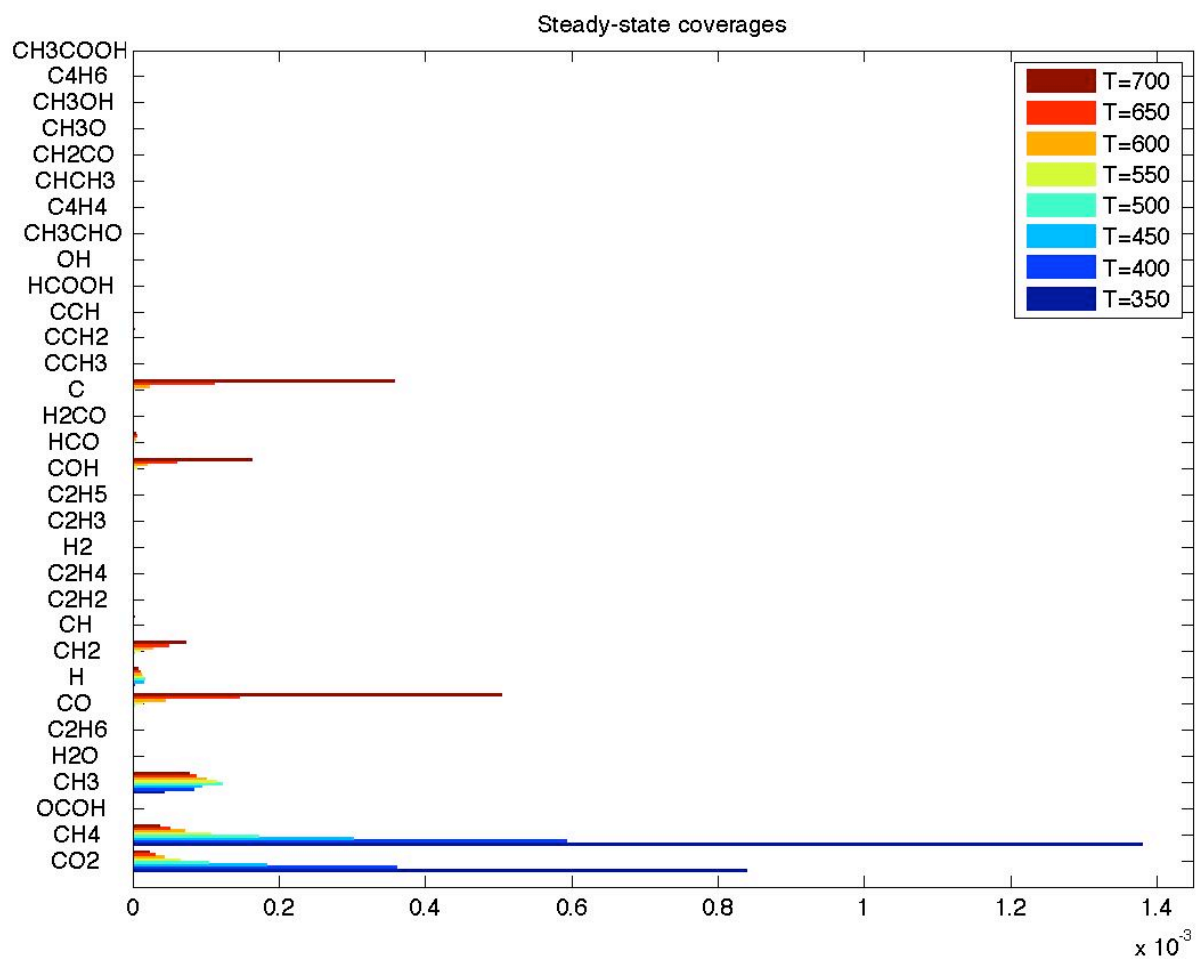


Figure 2. Log plot of the steady state coverages from 350K to 700K.

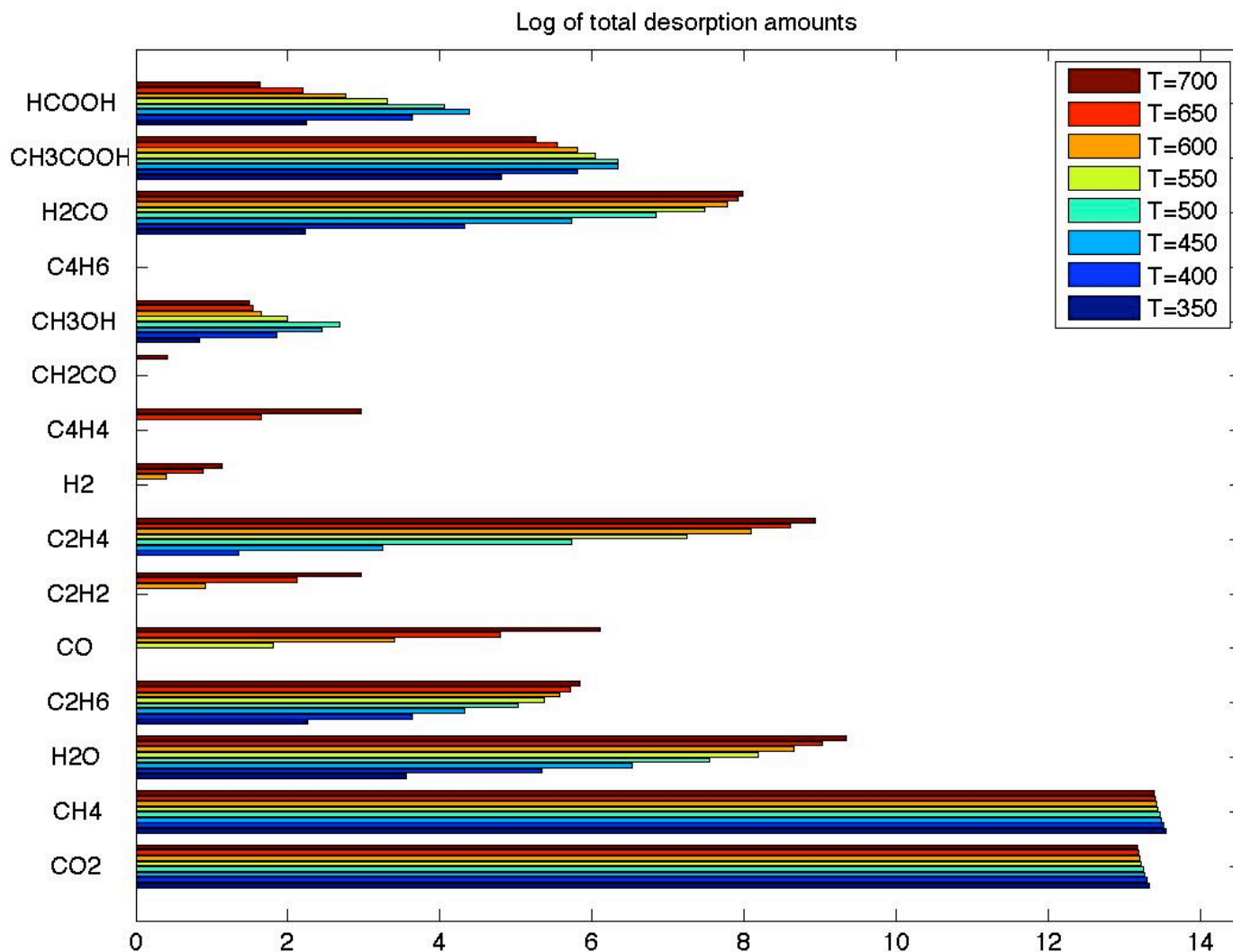


Figure 3. Log of total desorption amounts (coverage units) at one week of run-time.

The second hydrogenation of CO_2 to form formic acid can also occur along several reaction channels. The reaction channels that should be open are the addition of atomic hydrogen to OCOH and the disproportionation of OCOH with CH, generating atomic hydrogen on the surface. The lack of atomic carbon on the surface when formic acid coverage is relatively high is explained by the fact that the carbon dioxide is an

exceptionally good scavenger of atomic carbon. Carbon dioxide readily disproportionates with atomic carbon on the surface forming two carbon monoxide molecules. This atomic carbon scavenging by CO_2 is the reason why the surface does not become covered with carbon. Rezaei et al. [3] attributed the low efficacy of Pd for syngas production in part to carbon deposits on the surface. The feed gas employed in that work [3] did not contain CO_2 . In agreement with our results, Ding et al. [2] and Munera et al. [6] report a lack of carbon deposition or lack of a decrease in catalyst activity due to carbon deposition in their experiments with carbon dioxide over Pd.

Once formed, the formic acid on the surface can decompose to H and OCOH, disproportionate with a CH_x radical to form OCOH, or it may decompose to CO and OH. The latter reaction is not likely considering that the reverse of that reaction has a zero activation barrier.

A longer route to formic acid in terms of the overall number of steps is the pathway ending in the recombination of CO and OH. This pathway requires first the formation of CO, presumably from CO_2 and OH from either the dissociation of water or the disproportionation of atomic oxygen with a hydrogen source, such as CH_x or water. We consider this pathway to be an unlikely one and that the most active path likely involves first the hydrogenation of CO_2 by atomic hydrogen followed by the disproportionation of OCOH with CH forming atomic carbon on the surface that is quickly scavenged by CO_2 . Figure 2 indicates that the atomic hydrogen needed for the first hydrogenation of CO_2 is present. Also the methyl coverage is significantly greater than the atomic hydrogen

coverage, suggesting that much of the hydrogen generated from the dissociation of CH_4 has reacted.

The atomic carbon and CO coverages mirror each other as a function of temperature, and coverages of carbonaceous radicals are greater at higher temperatures, with the exception of the methyl radical, which participates in many reactions. The carbon monoxide coverage is due to the disproportionation of CO_2 with atomic carbon on the surface rather than CO_2 dissociation. The scavenging ability of CO_2 for adsorbed atomic carbon keeps the surface from becoming covered with the strongly bound atom. The absence of CH as a surface adsorbate is understood in light of the fact that the activation barrier for CH dissociation to C and H is only 5 kcal/mol. The coverages of the closed-shell molecules such as water, methanol, and molecular hydrogen are low due to the fact that they readily desorb.

The total desorption amounts of formic and acetic acid and methanol show peaks around the mid-range temperatures. Formaldehyde evolution is significant in the temperature range studied in this work and increases with temperature. At higher temperatures other reactions compete favorably and suppress the formation of methanol. Formic and acetic acid formation has been observed on Pd catalysts [2, 5]. In addition, Fujitani et al. have observed methanol and formaldehyde formation over supported palladium catalysts [15].

Figure 4 is analogous to Figure 3 with a total pressure of 600 kPa. The partial pressures of the methane and CO_2 are the same. Comparison of Figures 3 and 4 show slight

increases in total desorption amounts at the higher total pressure. Figure 5 is a graph of the total desorption amounts at a total pressure of one bar and an 80% / 20% feed gas mixture of CO₂ and methane. Figure 6 shows the total desorption amounts with an 20% / 80% feed gas composition. Certainly there will be a point at which the compounds desorbing will be drastically different, for example with a 100% / 0% mixture, but, when compared to the data in Figure 3, the data in Figures 5 and 6 show the sensitivity of the desorption amounts to the relative feed gas composition. There are changes in the desorption amounts with perhaps the most striking being the attenuation of the molecular hydrogen desorption and the C₂ hydrocarbon evolution with elevated CO₂ levels in the feed gas (Figure 5). As one might expect the data in Figures 5 and 6 indicate increased molecular hydrogen evolution and increased total desorption of the C₂ hydrocarbons when the feed gas is impoverished with respect to carbon dioxide.

The total desorption amounts of the oxygen-bearing species seem to be less sensitive although there are trends evident. Formic acid and water show a greater sensitivity to changes in partial pressures of the components in the feed gas than do formaldehyde, methanol, and acetic acid.

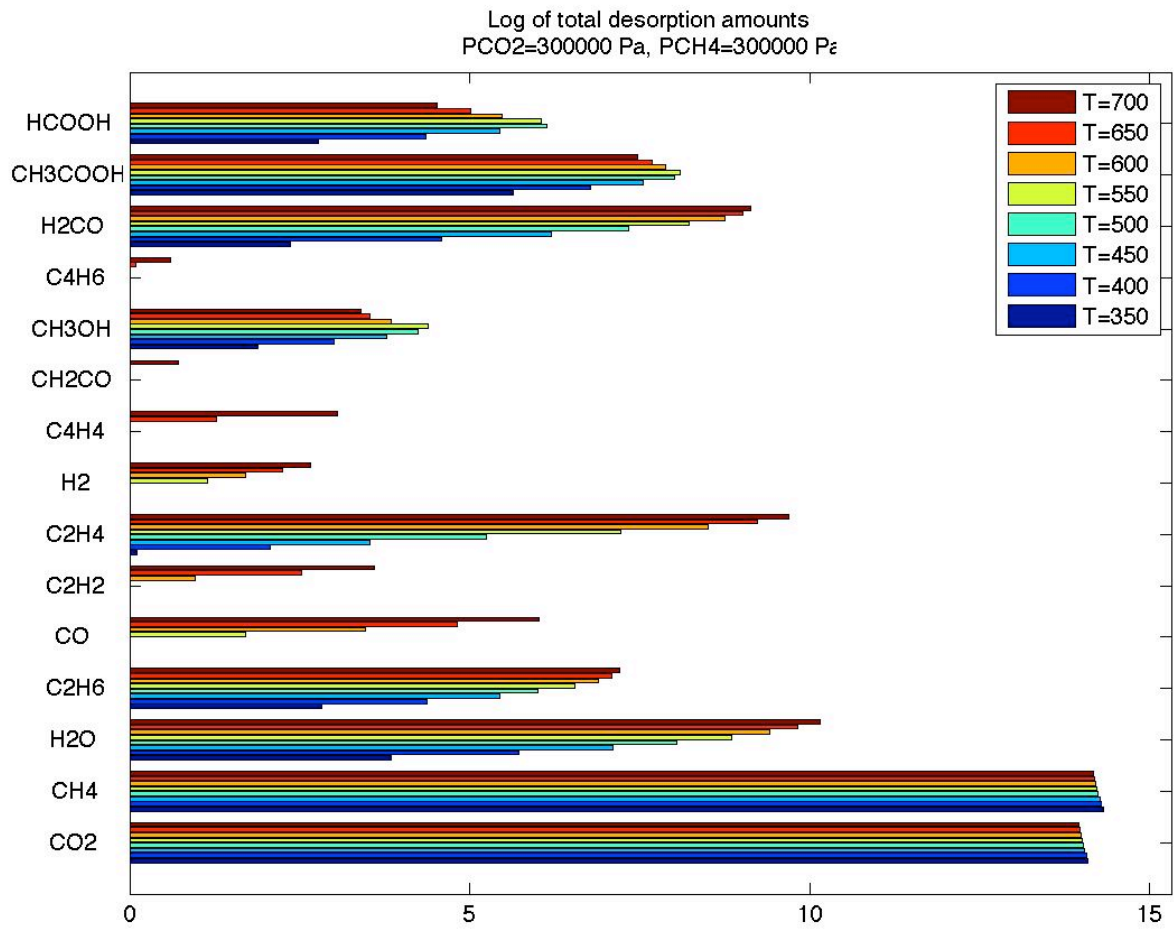


Figure 4. Total desorption amounts, total pressure = 600 kPa.

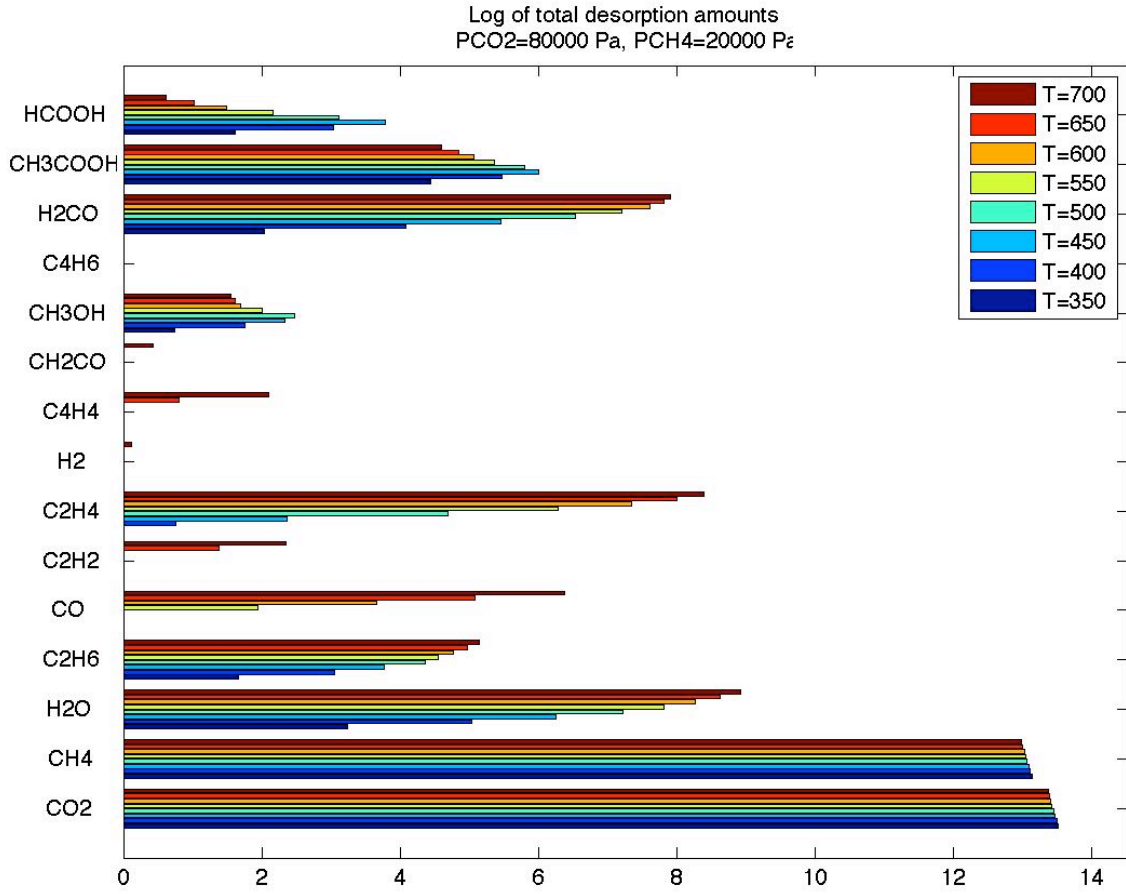


Figure 5. Total desorption amounts. Feed gas composition is 80% CO_2 and 20% CH_4 .

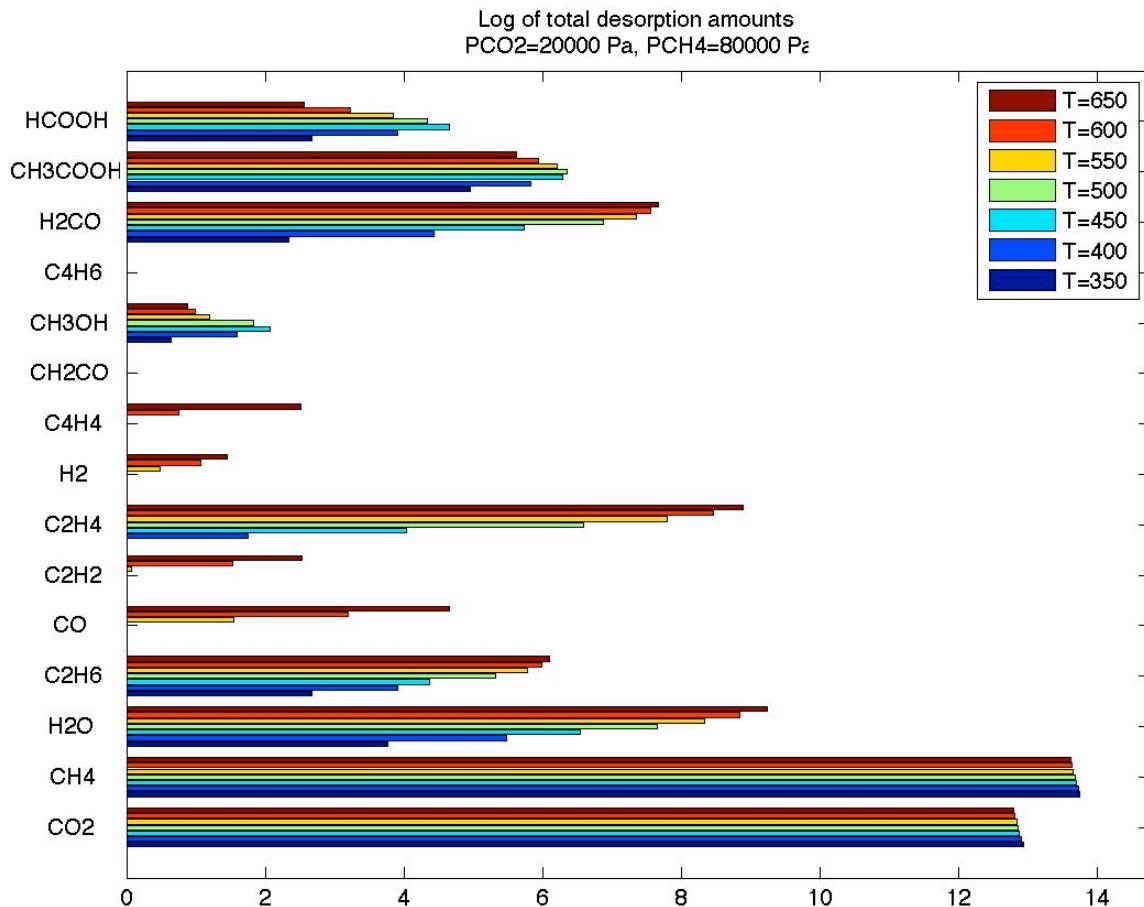


Figure 6. Log of total desorption. Feed gas composition is 20% CO₂ and 80% CH₄.

Judging from our results for the first differential slice of the plug flow reactor the conversion efficacy per differential slice is not high. For a palladium-based catalytic reactor to be an efficient converter of carbon dioxide and methane it would need to have thousands of differential slices. We are in the process of building a model of a much larger reactor. One of the goals of that work is to determine what is necessary for a reactor to be an efficient converter of carbon dioxide. In addition, our intent is to assess many other catalytic metals for efficacy in this regard.

Many of the products formed in this reactor, such as methanol, acetic acid, formaldehyde and others, are liquids at room temperature. Separating these product components from the effluent gas is relatively uncomplicated. Separating the gaseous components from each other will require gas separation techniques such as differential adsorption, membrane technology, methods that exploit diffusion rates and so on.

IV. Concluding remarks

The CO₂ / CH₄ system is relevant to important, current environmental issues. The flue gas of coal-fired electrical generating stations is almost entirely CO₂ while methane is available from the coal on site. The development and optimization of catalytic reactors that convert the carbon dioxide into non-greenhouse gases will make an important contribution to the technology of carbon sequestration. The compounds that we observe evolving from the catalyst surface, such as methanol, formaldehyde, C₂ hydrocarbons, and the components of synthesis gas have commercial value. The production and sale of these compounds will help offset the expense of carbon sequestration.

Herein we have developed a computational model the results of which are consistent with available experimental data with respect to the compounds produced. The formation of acetic acid, formic acid, methanol, water, molecular hydrogen, formaldehyde, and the C₂ hydrocarbons have been observed experimentally on supported palladium catalysts. We have shown that the distribution of reaction products is dependent on temperature, total pressure, and the partial pressures of the feed gas components. Our model corresponds to

the first differential slice of a plug flow reactor, and the chemistry of subsequent slices is expected to be similar. We are in the process of building a full reactor model for the treatment of flue gas emissions from the burning of fossil fuels.

References

1. S.V. Gredig, R.A. Koeppel, A. Baiker, *Cat. Lett.*, 46 (1997) 49.
2. Y.-H. Ding, W. Huang, Y.G. Wang, *Fuel Processing Technology* 88 (2007) 319.
3. M. Rezaei, S.M. Alavi, S. Sahebdehfar and Z.-F. Yau, *J. Mat. Gas Chem.* 15 (2006) 327.
4. S. Eriksson, M. Boatonnet and S. Jaras, *App. Cat. A: Gen.*, 312 (2006) 95.
5. E.M. Wilcox, G.W. Roberts, J.J. Spivey, *Cat. Today* 88 (2003) 83.
6. J. Munera, S. Irusta, L. Cornaglia and E. Lumbardo, *App. Cat. A: Gen.*, 245 (2003) 383.
7. E. Shustorovich and H. Sellers, *Surf. Sci. Rep.* 31 (1998) 1.
8. H. Sellers, *Russ. J. Phys. Chem. B*, Ed. by E. Shustorovich (Pleiades, Moscow, 2007), 1 (2007) 377.
9. H. Sellers, *J. Phys. Chem.*, 37 (2003) 10206.
10. H. Sellers and J. Gislason, *Surf. Sci.*, 426 (1999) 147.
11. I. Langmuir, *J. Am. Chem. Soc.*, 40 (1918) 1361.
12. I. Langmuir, *J. Am. Chem. Soc.*, 54 (1932) 2798.
13. L.F. Shampine and M.W. Reichelt, *SIAM J. Sci. Comput.*, 18 (1997) 1.
14. N. Aas, Y. Li, and M. Bowker, *J. Phys.: Condens. Matter* 3 (1991) S281.
15. T. Fujitani and I. Nakamura, *Bull. Chem. Soc. Japan*, 75 (2002) 1393.
16. H. Sellers, *Surf. Sci.*, 524 (2003) 29.